17th Australasian Fluid Mechanics Conference
Auckland, New Zealand
5-9 December 2010

# Flow Control Based on Three-Dimensional Wake Instabilities for a Blunt Trailing Edge Profiled Body

**A. Naghib-Lahouti, L.S. Doddipatla, and H. Hangan**

The Boundary Layer Wind Tunnel Laboratory
The University of Western Ontario, London, Ontario N6A 5B9, Canada

## Abstract

Flow in the wake of a blunt trailing edge profiled body has been studied experimentally at Reynolds numbers ($\mathrm{Re}(d) = U_\infty d/\nu$) ranging from 250 to 2000, based on the maximum thickness of the body ($d$), to identify and characterize the small-scale three dimensional instabilities in the near wake region.

Based on the findings concerning the small-scale instabilities, an active three-dimensional flow control mechanism has been developed and evaluated experimentally. The results indicate that the flow control mechanism is capable of reducing the mean and fluctuating components of drag using a small amount of secondary flow, when the spanwise excitation wavelength matches the natural spanwise wavelength of the small-scale instabilities.

## Introduction

Vortex shedding in the wake of nominally two-dimensional bluff bodies is known to be accompanied by large- and small-scale three-dimensional instabilities beyond a threshold Reynolds number. The large-scale instabilities appear as waves in the von Kármán vortices, leading to out-of-phase shedding at various spanwise locations, and the small-scale instabilities manifest as pairs of counter-rotating streamwise vortices, connecting the von Kármán vortices [1]. In the case of a circular cylinder, the instabilities initiate at Re(d)=194 with a mechanism known as Mode-A, in which waves in the von Kármán vortices in the near wake evolve into pairs of counter-rotating streamwise vortices which change sign every half shedding period. The spanwise wavelength of this instability is $\lambda_Z = 3d - 4d$. At Re(d)=230-260, this mechanism gradually gives way to the one known as Mode-B, in which the streamwise vortices appear with no sign change, with a smaller spanwise wavelength of $\lambda_Z = 1d$ [1].

The threshold Reynolds number, the order of appearance, and the spanwise wavelength of the small-scale instabilities is not unique for various bluff body profile geometries. For example, for the blunt trailing edge profiled body (Figure 1), which is the subject of the present study, the small-scale instability is predicted to appear at Re(d)=400 approximately, with a mechanism bearing general resemblance to Mode-A of a circular cylinder but with features specific to this geometry [2]. One of these specific features is the spanwise wavelength of the instability, which is predicted to be $\lambda_Z = 2.2d$, approximately. These predictions will be verified experimentally in the first part of the present study, through Laser Induced Fluorescence (LIF) flow visualizations, and velocity field measurements using Particle Image Velocimetry (PIV) and analysis using Proper Orthogonal Decomposition (POD).

Artificial excitation of the small-scale instabilities, which leads to disorganization of the von Kármán vortices, has been used as a means for reduction of the adverse effects of vortex shedding in several passive and active flow control approaches [3]. It is known that this approach is most effective when the excitation wavelength matches the wavelength of the small-scale instabilities ($\lambda_Z$) [4]. Based on this fact, and using the results obtained in the first part of the study, an active three-dimensional flow control mechanism is proposed. The flow control mechanism comprises a series of trailing edge injection ports, arranged with a spanwise wavelength equal to $\lambda_Z$ (Figure 2). The effectiveness of the flow control mechanism, and its effect on the wake flow structure have been investigated using multiple-plane PIV velocity field measurements and POD analysis in the second part of the study.

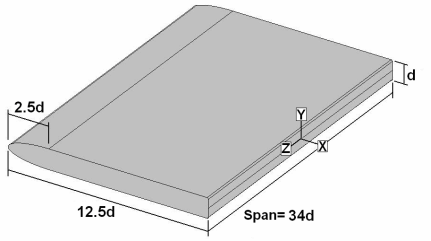


Figure 1. Geometry of the blunt trailing edge profiled body

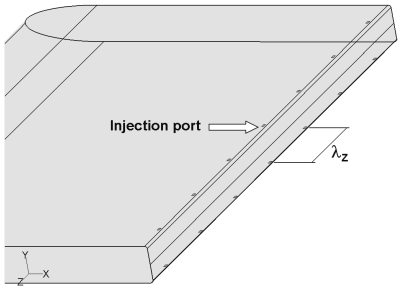


Figure 2. Schematic view of the flow control mechanism

## Experimental methodology

The experiments have been conducted in the closed test section open return water tunnel facility at the Boundary Layer Wind Tunnel Laboratory of the University of Western Ontario. The tunnel is capable of generating flow velocities up to 0.2m/s in a 0.6m(w)×0.3m(h) test section, with less than 1% velocity variation across the test section, and 0.1% free-stream turbulence intensity. The experimental model has a thickness of $d = 0.0127m$, and a chord to thickness ratio of 12.5. Blockage ratio based on the thickness of the model is 4.2%. Two end plates have been used to isolate the centre 34d portion of the span of the model from the boundary layer of the tunnel sidewalls and the secondary flow injection tubing.

LIF flow visualizations have been carried out using a Rhodamine 6G fluorescent dye solution, which was injected through a

spanwise slot located 1d upstream of the lower corner of the trailing edge, and illuminated using a 120mJ Nd-YAG pulse laser. The reflected laser light was filtered using a 550nm filter mounted in front of the objective lens of the CCD camera. In the flow control experiments, the slotted trailing edge was replaced with a trailing edge with an array of injection ports (Figure 2).

PIV velocity field measurements have been carried out using a CCD camera capable of capturing 15 image pairs per second with a resolution of 1600×1200 pixels, and the same laser used for the LIF experiments. 32×32 pixel interrogation windows with a 16-pixel overlap have been used to generate an array of 99×74 velocity vectors based on each image pair. For each experiment involving a particular measurement plane and Reynolds number, 3000 image pairs have been captured.

The velocity vector field data have been analysed using the Proper Orthogonal Decomposition (POD) technique described in [5]. This technique has been employed to establish a simplified reconstruction of the velocity field, which has then been used to identify the small-scale instabilities. In the flow control experiments, the technique has been used to study the role of the flow control mechanism in modal energy redistribution and reorganization in the near wake region.

The experiments have been carried out at Reynolds numbers ranging from Re(d)=250 to Re(d)=2150. However, only a selection of the results will be presented herein, to highlight the findings while observing the page limits of the proceedings.

## Results and discussion

Flow visualizations in the horizontal (XZ) plane located in-line with the lower corner of the trailing edge (y/d=-0.5) indicate that while the small-scale instabilities are observed occasionally at Reynolds numbers as low as Re(d)=400, their existence becomes persistent at and beyond Re(d)=550. This observation verifies the transition Reynolds number of Re(d)=475, predicted for the same geometry in [2].

Figure 3 shows an LIF flow visualization image captured at Re(d)=550. It can be observed in the figure that the small-scale instabilities initiate as waves in the von Kármán vortices (marked with (▷) symbols), which evolve into pairs of counter-rotating streamwise vortices (marked with (◁) symbols) further downstream, in a mechanism generally similar to that of Mode-A of a circular cylinder. One interesting feature observed in Figure-3 is the anti-symmetric behaviour of the waves in the von Kármán vortices in the near wake region, which appears as switching of the locations of peaks and valleys in the two consecutive von Kármán vortices shed from the same corner of the trailing edge. This observation is consistent with the "wake reversal" characteristic of the same geometry, first reported in [2].

Considering the correlation between the spanwise wavelength of the small-scale instabilities ($\lambda_z$) and the spanwise variations of streamwise velocity component ($u$) [6], PIV measurements of the streamwise velocity field in the near wake region have been used to determine the average value of $\lambda_z$. To facilitate the identification of the instabilities, POD analysis has been used to reconstruct the spatial and temporal variations of the velocity field. Figure 4 shows an example of the spanwise and temporal variations of the streamwise velocity component ($u$) at Re(d)=550, reconstructed using the first 32 POD modes, which contain 80% of the relative cumulative energy of the original data ensemble. The average wavelength ($\lambda_z$), determined based on superposition of the first 32 POD modes of $u$, is found to be 2.0d at Re(d)=550, 2.4d at Re(d)=850, and 2.5d at Re(d)=1200 and 2150. These values are in reasonable agreement of the predicted value of $\lambda_z$=2.2d, reported in [2].

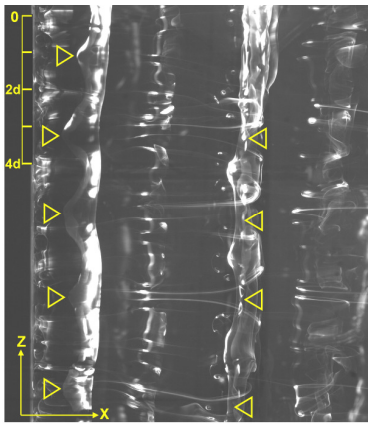


Figure 3. Flow visualization in the XZ plane at y/d=-0.5, at Re(d)=550

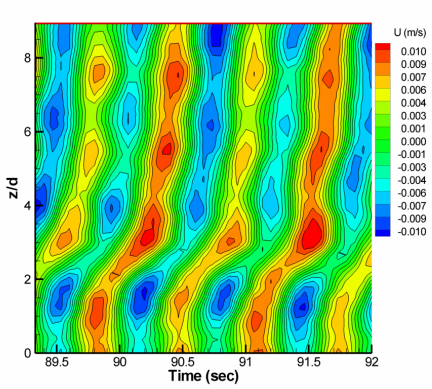


Figure 4. Spatial and temporal variations of streamwise velocity ($u$) at x/d=2.0, y/d=0.5, based on the first 32 POD modes, at Re(d)=550

The flow control experiments have been conducted using a secondary flow injection rate of $u_i/U_\infty = 2.0$, which is equivalent to a control momentum coefficient of $C_\mu = 1\%$, as defined in equation (1):

$$C_\mu = \frac{2\rho u_i^2 n a_i}{\rho U_\infty^2 b d} \qquad (1)$$

In equation (1), $a_i$ is the area of each injection port, $n$ is the number of injection ports, $b$ is the span and $d$ is the thickness of the profiled body.

The effectiveness of the flow control mechanism in drag reduction, and its effect on the wake flow structure have been studied at Re(d)=700, 815, 1280, and 1980. At each Reynolds numbers, 4 sets of vertical (XY) plane PIV measurements have been carried out. One set corresponds to the base (no injection) case, and the other three sets, in which the control mechanism has been operative, correspond to three vertical planes located at $z/d = 0$, $z/d = \lambda_z/4$, and $z/d = \lambda_z/2$, measured from the injection port located at the mid-span (Figure 5). A selection of the results of these measurements will be presented in the following paragraphs to highlight the findings of the flow control experiments.

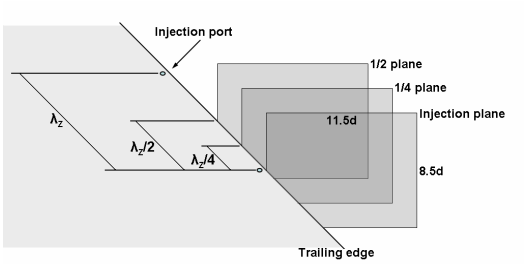


Figure 5. Schematic drawing showing the location of the three PIV measurement planes in the flow control experiments

Profiles of the mean and fluctuating components of streamwise velocity ($\overline{u}$ and $u_{rms}$) have been used to determine the effect of the flow control mechanism on the mean and fluctuating components of drag, which are given by the first and the second term of equation (2), respectively:

$$C_D = \frac{2}{A}\int_W \frac{\overline{u}}{U_\infty}\left(1-\frac{\overline{u}}{U_\infty}\right)dy + \frac{2}{A}\int_W \left(\frac{u_{rms}}{U_\infty}\right)^2 dy \qquad (2)$$

In the above equation, which is based on the methodology presented in [7], $A = bd$ is the frontal area of the body.

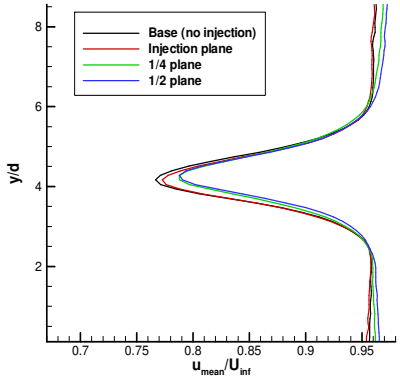


Figure 6. Profiles of normalized mean streamwise velocity at x/d=11.5 in multiple measurement planes at Re(d)=1280, compared with the base case

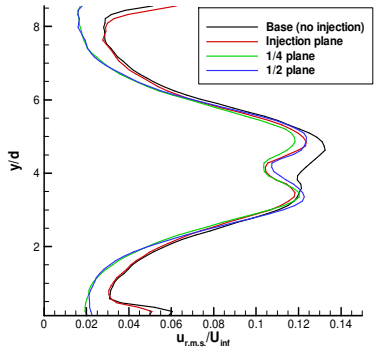


Figure 7. Profiles of normalized fluctuating streamwise velocity at x/d=11.5 in multiple measurement planes, at Re(d)=700, compared with the base case

The results indicate that the maximum reduction of the first term of equation (2) by the flow control mechanism is 10%, which has been achieved at Re(d)=1280. The maximum reduction of the second term is 14%, at Re(d)=700. Profiles of $\overline{u}$ and $u_{rms}$ at x/d=11 are shown in Figures 6 and 7 for Re(d)=1280 and 700, respectively.

The drag reduction obtained by controlling the flow in the near wake region of a bluff body with forced shear layer separation, such as the one studied herein, is known to be accompanied by a decrease in the minimum wake width, and an increase in the length of the vortex formation region [8]. The length of the vortex formation region is defined as the location along the wake centreline where $u_{rms}$ reaches a maximum, and wake width is defined as the vertical distance from the wake centreline where $\overline{u}$ reaches $0.9U_\infty$.

The effect of the flow control mechanism on the minimum wake width is most evident at Re(d)=1280, where the maximum reduction of the first term of equation (2) is achieved (Figure 8), and the effect of the flow control mechanism on the length of vortex formation region is most evident at Re(d)=700, where the maximum reduction of the second term of equation (2) is achieved (Figure 9). Similar behaviours have been observed at the other Reynolds numbers investigated herein, albeit with different intensities.

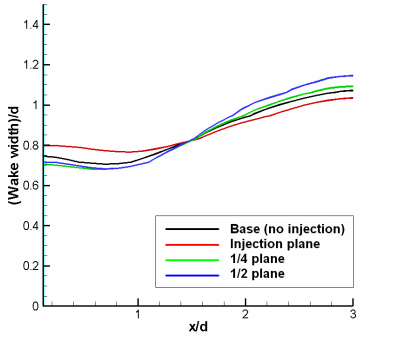


Figure 8. Variations of wake width in multiple measurement planes, compared with the base case, at Re(d)=1280

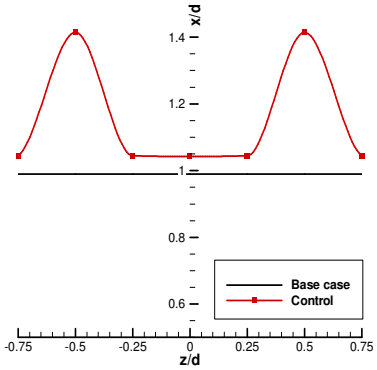


Figure 9. Effect of the flow control on the length of vortex formation region at various spanwise locations, at Re(d)=700

The flow control mechanism also causes a reduction of maximum amplitude in the frequency spectra of both streamwise and vertical velocity components in all measurement planes. An example of this effect, which is associated with the attenuation of the fluctuating component of drag force through equation (2), is shown in Figure 10 for Re(d)=815.

Finally, the effect of the flow control mechanism on relative energy contained by the von Kármán vortex street and the small-scale instabilities can be investigated by comparing the relative

energies of POD modes in the vertical (XY) plane, with and without flow control, shown in Figure 11. The first two POD modes are known to be associated with the von Kármán vortices [9], while the higher POD modes are associated with the the small-scale instabilities, as well as the harmonics of the first two POD modes. The flow control mechanism causes a reduction of the relative energies of the first two POD modes, and an increase in the relative energies of the higher POD modes in all measurement planes, as exemplified in Figure 11 for Re(d)=815. This behaviour suggests that the flow control mechanism generates its previously described effects through amplification of the small-scale instabilities, leading to reduction of the energy of the von Kármán vortices.

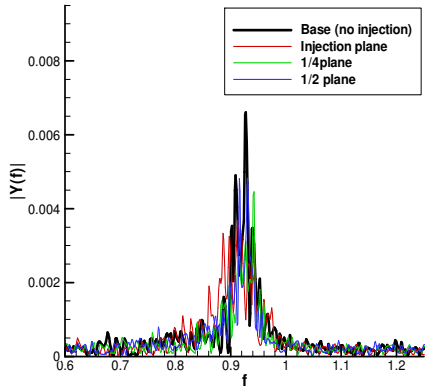


Figure 10. Effect of the flow control on frequency spectra in multiple measurement planes, compared with the base case, at Re(d)=815

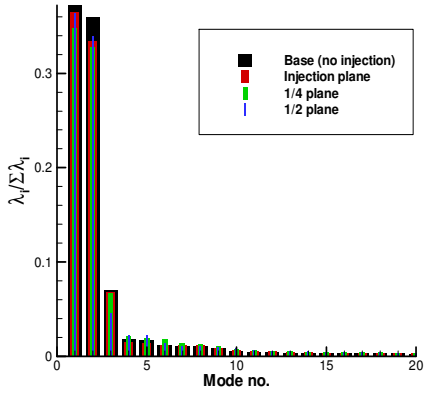


Figure 11. Effect of the flow control on relative energy of POD modes in multiple measurement planes, compared with the base case, at Re(d)=815

## Conclusions

The flow structure in the wake of a blunt trailing edge profiled body has been studied experimentally at Reynolds numbers ranging from Re(d)=250 to Re(d)=2150, in order to identify the small-scale three-dimensional instabilities accompanying the von Kármán vortex street. The results indicate the existence of a prominent small-scale instability with a spanwise wavelength of $\lambda_z = 2.0d - 2.5d$, having a mechanism generally similar to that of Mode-A wake instability of a circular cylinder, with features specific to the blunt trailing edge profiled body. These findings verify the predictions by Ryan et al. [2] for the same geometry.

Based on the findings about the small-scale instability, an active three-dimensional flow control mechanism has been designed and evaluated experimentally. The results of the flow control experiments indicate that the proposed flow control mechanism is able to generate a maximum reduction of 14% in the fluctuating component of drag, and a maximum reduction of 10% in total drag, by amplifying the small-scale instabilities, using a small amount of secondary flow.

## Acknowledgment

The authors would like to express their gratitude to Dr. Kamran Siddiqui, associate professor at the Department of Mechanical and Materials Engineering of the University of Western Ontario, for providing the visualization and image recording apparatus, and his expert advice during the LIF and PIV experiments.

## References

[1] Williamson, C.H.K., Vortex Dynamics in the Cylinder Wake, *Annu. Rev. Fluid Mech.*,**28**, 1996, 477-539.

[2] Ryan, K., Thompson, M.C., & Hourigan, K., Three-dimensional Transition in the Wake of Bluff Elongated Cylinders, *J. Fluid Mech.*, **538**, 2005, 1-29.

[3] Choi, H., Jeon, W.P., & Kim, J., Control of Flow over a Bluff Body, *Annu. Rev. Fluid Mech.*, **40**, 2008, 113-139.

[4] Darekar, R.M. & Sherwin, S.J., Flow past a Square-Section Cylinder with a Wavy Stagnation Face, *J. Fluid Mech.*, **426**, 2001, 263-295.

[5] Smith, T.R., Moehlis, J. & Holmes, P., Low-dimensional Modelling of Turbulence using Proper Orthogonal Decomposition, *Non-linear Dynamics*, **41**, 2005, 275-307.

[6] Wu, J., Sheridan, J., Welsh, M.C. & Hourigan, K., Three-dimensional Vortex Structures in a Cylinder Wake, *J. Fluid Mech.*, **312**, 1996, 201-222.

[7] Van Oudheusden, B.W., Scarano, F., Roosenboom, E.W.M., Casimiri, E.W.F. & Souverein, L.J., Evaluation of Integral Forces and Pressure Fields from Planar Velocimetry Data for Incompressible and Compressible Flows, *Exp. Fluids*, **43**, 2007, 153-162.

[8] Bearman, P.W., Investigation of Flow behind a Two-dimensional Model with a Blunt Trailing Edge and Fitted with Splitter Plates, *J. Fluid Mech.*, **21**, 1965, 241-255.

[9] Deane, A.I., Kevrekidis, I.G., Karniadakis, G.E. & Orszag, S.A., Low-dimensional Models for Complex Geometry Flows, *Phys. Fluids*, **3**, 1991, 2337-2354.